ELSEVIER

Physica B 281&282 (2000) 716–722

PHYSICA B

www.elsevier.com/locate/physb

Invited Paper

Advances in photoemission spectroscopy of f-electron materials

J.D. Denlinger[a,*], G.-H. Gweon[a], J.W. Allen[a], C.G. Olson[b], Y. Dalichaouch[c], B.-W. Lee[c], M.B. Maple[c], Z. Fisk[d], P.C. Canfield[b], P.E. Armstrong[e]

[a]*Department of Physics, University of Michigan, Ann Arbor, MI 48109-1120, USA*
[b]*Ames Laboratory, Iowa State University, Ames, IA 50011, USA*
[c]*Department of Physics, University of California at San Diego, La Jolla, CA 92093, USA*
[d]*NHMFL, Florida State University, Tallahassee, FL 32306, USA*
[e]*Los Alamos National Laboratory, Los Alamos, NM 87545, USA*

Abstract

The recent capability to perform angle-resolved photoemission spectroscopy (ARPES) with improved energy and angle resolution over a wide photon energy range has provided new information about f-electron systems. Results for two rather different systems, 5f-electron heavy fermion metal URu_2Si_2 and 4f-electron mixed-valent SmB_6 are compared and contrasted.

Keywords: f-electron; Angle-resolved photoemission; URu_2Si_2; SmB_6; d–f hybridization

1. Introduction

The mixed valent and heavy-fermion properties of f-electron materials force one to confront the quintessential and still unsolved problem of electrons in solids — the tension between atomic and electron gas physics. It has been appreciated since the early 1980s that this is generally not an "either/or" question, i.e. for a single material, some properties, e.g. Kondo effects, can be described by single-ion f-electron models and yet the f-electrons contribute to the Fermi surface (FS) [1]. Electron spectroscopy has been very successful in revealing single-ion properties [2,3], while quantitative FS information has been obtained only by magneto-oscillatory (MO) techniques such as the de Haas–van Alphen (dHvA) effect [4–6]. MO techniques do not provide a global view of the energy and k-dependence of the electronic structure, and so are limited for distinguishing different theoretical scenarios of heavy-mass FS formation. Angle-resolved photoemission spectroscopy (ARPES) in principle provides this global view and some pioneering studies have been performed [7–9]. But because of technical barriers, ARPES has never provided enough FS details in these systems for its potential to be realized.

The barriers to serious ARPES studies of heavy-fermion systems are many and severe. (a) The simplest model expression relating the quasi-particle effective mass m^* to the slope of the quasi-particle dispersion at the Fermi wave vector k_F is $m^* = \hbar^2 k_F/(\partial E/\partial k)$. Taking $k_F \approx 0.5\ \text{Å}^{-1}$ yields $\partial E/\partial k = 3.81/(m^*/m_e)\ \text{eV/Å}^{-1}$ and for an m^* of e.g. $50m_e$ one has $\partial E/\partial k \approx 0.075\ \text{eV/Å}^{-1}$. For an interval near k_F even as large as $\delta k \approx 0.1\ \text{Å}^{-1}$ the dispersion is less than $\delta E \approx 7.5$ meV. Alternatively, impurity Kondo models suggest energy scales δE ranging from 10 to 1 meV or less for (m^*/m_e) ranging upward from ≈ 50, implying extremely small δk. Ideally, the k and E resolutions should be even smaller, say 20% of the relevant δk and δE ranges. To have Fermi function broadening $\approx 4k_BT <$ e.g. 5 meV requires $T < 14$ K. (b) Most materials are three dimensional and hence require tunable photon energies to access the full Brillouin zone since ARPES measurements at constant photon

* Corresponding author. Present address: MS 7-222, Lawrence Berkeley National Laboratory, 1 Cyclotron Road, Berkeley, CA 94720, USA. Tel.: +1-510-486-5648; fax: +1-510-486-7588.

E-mail address: jddenlinger@lbl.gov (J.D. Denlinger)

0921-4526/00/$ - see front matter
PII: S0921-4526(99)00915-1

energy traverse k-space along spherical arcs. Determination of the component of $\boldsymbol{k}$ perpendicular to the sample surface while moving on these arcs requires modeling of the surface potential step with an inner potential [10]. The photoelectron lifetime causes relaxation of k-perpendicular conservation which results in k_z-broadening [11] that further complicates the measurement of three-dimensional Fermi surface and band structure topologies [12,13]. On the positive side, the very small dispersion for an isolated heavy band could minimize the concomitant contribution [11] to the photohole line width. (c) Testing models of heavy-mass formation requires identifying f-character through the photon energy dependence of the f-cross section, e.g. by resonant photoemission spectroscopy (RESPES) [14]. (d) It can be important to distinguish surface and bulk contributions to the spectra, utilizing the angle and kinetic energy dependences of the probe depth [15–17]. The latter again involves changing the photon energy. The photon energy and angle variations of (a) through (d) all interact.

Recent advances in photoemission instrumentation and techniques have led to progress in these challenges for studying f-electron materials. Energy resolution will always be the smallest at low photon energy due to the narrow line widths of gas-discharge resonance lamps and/or the scaling of resolution with constant resolving-power monochromators and detectors. Recent achievement of 5–8 meV total instrumental resolution [9,18] has been aided by the use of a Scienta SES-200 electron energy analyzer and a high-flux GAMMADATA discharge lamp combined with low sample temperatures (< 13 K). Increases in detector resolution and efficiency have been made possible by the improvements in the stability of voltage power supplies and the use of multichannel detection systems. These laboratory-based experiments make use of differential excitation cross sections at He I and He II photon energies, 21.2 and 40.8 eV, respectively, to distinguish f-character. In contrast, at higher photon energies, where the $4d \rightarrow 4f$ rare earth and $5d \rightarrow 5f$ actinide resonances around 100–150 eV are used to distinguish f-character, it has been the photon source and not the detector that has limited the total energy resolution. The photon flux achievable for narrow slit settings of constant resolving-power monochromators at synchrotron sources has limited usable photon resolutions to typically ~ 50 meV at 100 eV and > 0.5 eV at 1000 eV. Increased flux from newer undulator-based beamlines has recently improved these resolutions by approximately a factor of five [19].

Since ARPES is inherently an order of magnitude less efficient in its detection than angle-integrated photoemission, the increase in flux allows ARPES to be performed at higher photon energies with energy and angle resolutions previously only achievable at low photon energy. This allows the combination of resonant photoemission and ARPES to probe the lattice effects of the f-spectral weight. Also, since the basic quantum of data in an ARPES experiment is typically not a single spectrum, but a sequence showing spectral changes with $\boldsymbol{k}$, increases in the speed of data acquisition due to flux enhancement and multi-channel detection efficiency have been important. In particular, a new angular-mapping mode introduced in the Scienta 2D-detection system has now made an angular series of spectra the basic unit of data acquisition. In addition, the much lower angular resolutions of 0.2° achievable with this system, compared to $\pm 1^\circ$ in typical low-energy ARPES experiments, will greatly enhance ARPES in k-resolution limited systems and make true spectral line shapes experimentally accessible. For comparison, analyzer angular resolutions of $\pm 0.1^\circ$ and $\pm 1^\circ$ at photon energies of ~ 20 (120) eV correspond roughly to k-resolutions of 0.01 (0.02) and 0.1 (0.2) Å^{-1}, respectively.

Finally, the introduction of the "Fermi-surface mapping" technique [20–23], allows a more global view of the k-space variations in an ARPES experiment. In this technique, which is just a reapplication of core-level photoelectron diffraction experimentation to valence-band studies, the photoemission intensity within a constant kinetic energy window is acquired as a function of sample or detector angle and/or photon energy, thereby highlighting the passing (or close approach) of bands through this energy window. With the energy window set at the Fermi level, the resulting intensity modulations signify the k-space location of the approach or crossing of dispersing bands. With sufficient accounting of energy and k-resolutions, Fermi surface dimensions can experimentally be determined for certain systems. Acquisition of this global E_F-intensity map, which also provides information on sample alignment, matrix element and polarization effects, is very useful in instructing the experimentor where to focus attention with more detailed high-resolution spectra.

In this paper, we use two contrasting f-electron systems, URu_2Si_2 and SmB_6, to illustrate the advancements in (i) improved energy and angular resolution, (ii) higher flux and detection efficiency and (iii) the use of E_F-intensity mapping techniques over an exceptionally wide photon energy range. SmB_6 is a cubic mixed-valent and probably small-gap 4f system, and URu_2Si_2 is a heavy-fermion superconducting 5f system for which band calculations and dHvA data are available. We have been able to obtain very interesting new information even though our resolutions and sample temperatures in the data presented are not the ultimate state-of-the-art as listed above and are only approaching what is really required for these materials.

Results presented were obtained at two synchrotrons with three different endstations. Low photon energy (14–34 eV) experiments were performed at the SRC Ames/Montana beamline with fixed sample/moveable detector geometry with energy and angular resolutions of

$\Delta E = 50$–100 meV, $\Delta\theta = \pm 1^\circ$, and a sample temperature of $T_S \approx 25$ K. Medium photon energy (30–140 eV) experiments were performed at the SRC PGM undulator beamline employing a Scienta 200 analyzer with $\Delta E = 20$ meV, $\Delta\theta = 0.36^\circ$ in an energy/angular imaging mode and $T_S \approx 20$ K. High photon energy (80–200) experiments were performed at the ALS undulator beamline 7.0 employing a high-flux narrow-focus (100 μm) beam spot and a fixed detector/rotating sample geometry with 16-energy channel parallel detection, $\Delta E = 60$ meV, $\Delta\theta = \pm 0.7^\circ$ and $T_S \approx 150$ K. Samples were cleaved in vacuum exposing the [0 0 1] surface at $T_S < 25$ K for He refrigerator cooling at the SRC and at room temperature at the ALS. The single crystals of SmB_6 and URu_2Si_2 were prepared from an aluminum flux, and from an arc-cast polycrystalline rod by zone melting in high vacuum, respectively.

2. URu_2Si_2

URu_2Si_2 is a paramagnet with a moderately large specific heat coefficient of $\gamma \sim 65$ mJ/mol K^2 [24] that undergoes antiferromagnetic ordering at 17.5 K and then becomes superconducting at 1.2 K [25]. A change in γ through the antiferromagnetic transition might signal an important change in the Fermi surface, although our data up to now are in the paramagnetic phase and so do not address this aspect. Additional interest in this material results from evidence for the coexistence of antiferromagnetism and superconductivity, properties generally thought to be mutually exclusive. Also, the Ce analog to this compound, $CeRu_2Si_2$, is well known in the literature for excellent agreement between dHvA measurements and renormalized band theory, i.e. the number, size and effective masses of Fermi surface orbits well accounts for its T-linear specific heat value of ~ 350 mJ/mol K^2 [5,26].

The E_F-intensity mapping technique is demonstrated for URu_2Si_2 in Fig. 1. A k_X–k_Z slice in the [1 0 0] plane, displayed in Fig. 1(a), is obtained by recording the photoemission intensity in a 0.1 eV wide energy window centered on the Fermi level as a function of one detector angle (in the plane of photon polarization) and the photon energy $h\nu$ (varied from 14 to 34 eV). The dominant feature observed is a bright intensity at normal emission at $h\nu = 18$ eV. With an inner potential of 12 eV, chosen to align this feature to Γ at the center of the body-centered tetragonal Brillouin zone (BZ), we additionally observe alignment of bright intensities at Γ and Z in the second Brillouin zones. The fact that there is distinct intensity modulation as a function of k_Z is encouraging that the k_Z-broadening does not average the entire BZ. A dual-angle map at a fixed $h\nu = 18$ eV, displayed in Fig. 1(b), measures on a hemispherical surface in k-space and is presented as an image projected onto

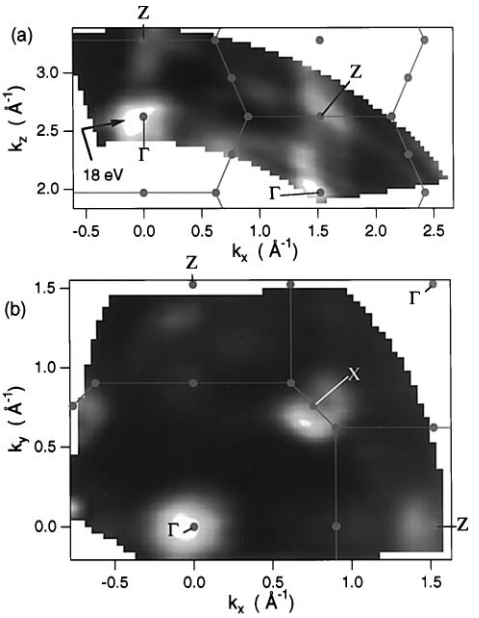

Fig. 1. Fermi-edge intensity maps of URu_2Si_2 used to identify the major regions of k-space involved in the Fermi surface: (a) k_X–k_Z slice in the [1 0 0] plane performed by varying one detector angle and the photon energy from 14 to 34 eV; (b) angular map at 18 eV projected onto the k_X–k_Y plane. An inner potential of 12 eV is determined from the k_X–k_Z map.

the k_X–k_Y plane, plotted with the BZ boundaries for $k_Z = 0$. In addition to the bright Γ-point intensity at normal emission, weaker intensities corresponding to near-Γ in the second BZs (follow 18 eV arc of Fig. 1(a) to near-Γ below Z) are observed as well as a ring of intensity at the point labeled X (Fig. 1(b)). Because of the curved k-space arc of the measurement, we can make only the initial claim that this ring structure is centered at a k-parallel position corresponding to the vertical P–X–P line. This feature, which we will refer to as the X-point, is discussed in more detail below.

While measurement of spectra as a function of $h\nu$ at normal emission, traversing –Γ–Z–Γ–Z-, tends always to show a resolution-limited peak very close to E_F, the Γ-point can be distinguished from the Z-point by additional spectral weight at ≈ 0.6 eV binding energy and is observed at 18, 56, 97, 156 and 220 eV, confirming the choice of inner potential. Measurement of spectra as a function of angle in high symmetry planes at low and high photon energy reveals the major FS intensity maxima to originate from hole-like dispersions. Rapid acquisition of spectra to 4 eV binding energy with finely stepped angles (0.5°) allows imaging of continuous band maps as illustrated in Fig. 2(a) for $h\nu = 125$ eV where normal emission corresponds to the Z-point and $h\nu$ is just above the 5d → 5f RESPES maximum at 108 eV.

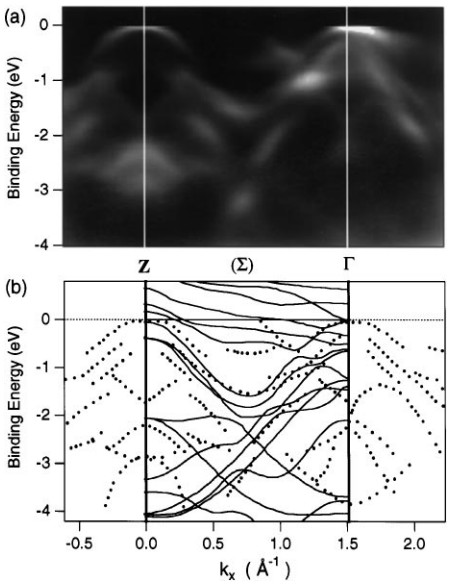

Fig. 2. (a) Normalized intensity plot of URu_2Si_2 (0 0 1) spectra at $h\nu = 125$ eV for emission angles in the [1 0 0] plane. (b) Comparison of experimental bands (dots) to the calculated band structure along Z–(Σ)–Γ (lines [27]).

Normalization of the intensity modulation in this image has been chosen to enhance the weaker band dispersions at deeper binding energies. No evidence for valence-band Auger decay is observed in valence spectra at or above this 5d → 5f absorption edge.

At larger $h\nu$, the k-space arc curvature and k_Z variation is less. Hence the k-space trajectory for Fig. 2(a) cuts close to Γ in the second BZ and so is a reasonable approximation to the Z–(Σ)–Γ line for which band structure calculations are available. Fig. 2(b) shows a comparison of the experimental band dispersion from Fig. 2(a) (dots) to a calculated band structure for URu_2Si_2 in the paramagnetic regime [27]. We observe agreement with many of the bulk band dispersions, in particular with the parabolic band that is symmetric between Z and Γ, has a band minimum at $\sim$1.5 eV and then flattens out at the Z and Γ points. However, the agreement with band crossings that form the Fermi surface is much less. Band calculations [27–29] predict 2–3 concentric hole surfaces at the Z-point, while experimentally, only a single small hole-pocket, coincident with strong f-weight, is observed. At the Γ-point, strong f-weight coincident with a hole-like dispersion is also observed, but detailed spectra give evidence of a finite binding energy and so perhaps a lack of Fermi surface. A large electron-like surface centered on Γ is calculated and experimentally a large electron-like dispersion crosses near half-way from Γ–Z, but with a much larger dispersion than in the calculation. In addition, calculations predict at the X-point either no Fermi surface or a small electron pocket whereas experimentally a hole surface is distinctly observed, as shown below in Fig. 4.

Fig. 3. shows two E_F-intensity angular maps, one below the 5d → 5f resonance at 85 eV where one expects predominant Ru 4d-character and one above the resonance at 112 eV where U 5f weight is enhanced. Data were acquired over a 90° sector and then four-fold symmetrized, and are presented in a split fashion with BZ boundaries for $k_Z = 0$ similar to Fig. 1. The general impression from the two E_F-intensity maps is the hint of small closed topologies of Fermi surface at high-symmetry k-parallel points below resonance, with intensity filling in these topologies above resonance. We focus our attention on these closed FS topologies, most notably the diamond-shaped ring at the X-point similar to that observed at 18 eV in Fig. 1(b), and do not attempt to interpret the other intensity maxima which require additional experiments to explore their origin. The observation of closed FS topologies suggests making comparison with the sizes of Fermi surface orbits measured in MO experiments. Representative sizes of circular orbits corresponding to measured Shubnikov–de Haas frequencies in the antiferromagnetic phase [30] are shown in Fig. 3(b). Qualitatively by eye, the two larger orbits have a possible correspondence to the diamond-shaped feature at X and the larger structure at Z, and the smaller orbits have potential matches to the small hole pockets at Z and Γ observed in Fig. 2. However, quantitative comparison requires establishing a correspondence between the map

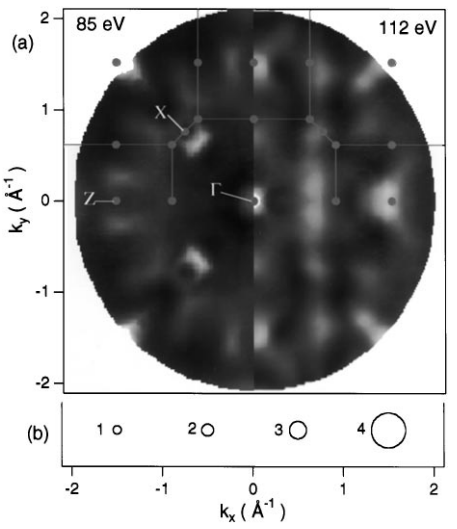

Fig. 3. (a) E_F-intensity angular maps of URu_2Si_2 (0 0 1) at two photon energies, (left) below resonance at 85 eV and (right) above resonance at 112 eV. (b) Representative sizes of four Fermi-surface orbits measured in the antiferromagnetic phase by magnetoresistance [30].

intensities and E_F-crossings determined from detailed spectra. Also, further comparison to dHvA awaits future ARPES experiments performed below 17.5 K in the antiferromagnetic phase.

Next, we explore the X-point FS structure in detail. Zoomed images of the X-point from Fig. 3 are shown in Fig. 4(a) and (b) to highlight this effect of on-resonance f-weight filling in an off-resonance closed orbit of d-character. Spectra taken along the diagonal line shown in Fig. 4(a) at the same photon energies as the maps are shown in Fig. 4(c) and (d). The hole-like dispersion of this piece of Fermi surface is clearly evident at both energies. Consistent with the E_F-intensity maps, above resonance a sharp E_F-peak which we attribute to U 5f weight is enhanced in the interior of the hole-pocket. The two sequences of spectra are scaled to have equal E_F-intensity away from the hole-pocket in order to compare relative intensities of spectral features. The intensities of the dispersing bands are significantly diminished from 85 to 112 eV, qualitatively consistent with the broad Cooper minimum around 105 eV in the cross section of Ru 4d electrons. There also appears to be a strong and varying asymmetry in the relative strengths of the two dispersing bands as a function of $h\nu$ as illustrated in the k_X–k_Z E_F-intensity map in Fig. 4(e). This k_X–k_Z image has been normalized by an angle-integrated intensity profile in order to remove the strong overall f-resonance and highlight the relative intensities of the edges and interior of this structure which extends along the P–X–P line. The maps and spectra acquired at 85 and 112 eV are observed to cut close to the P-points.

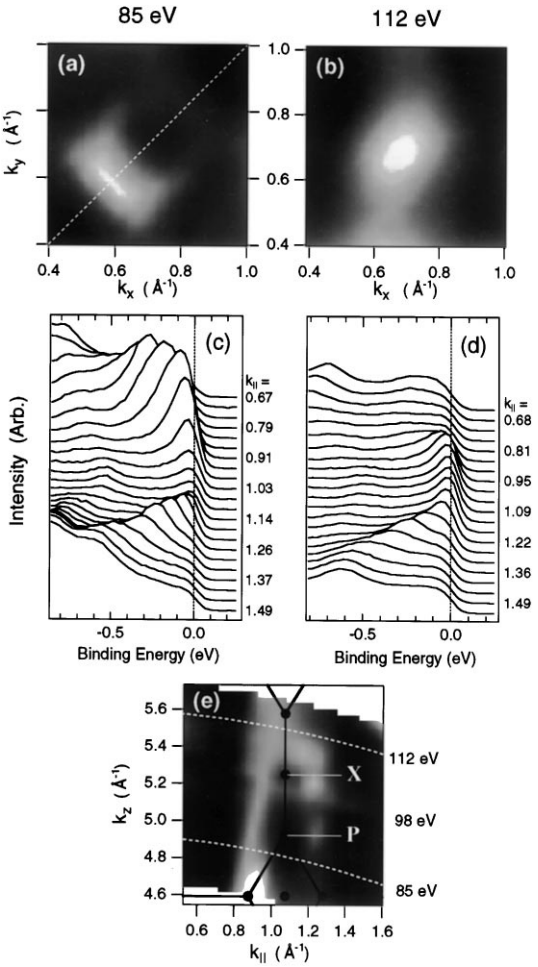

Fig. 4. (a, b) Zoomed k_X–k_Y E_F-intensity maps of the X-point at 85 and 112 eV. (c, d) Spectra taken along the diagonal trajectory showing hole-like dispersions. (e) A k_X–k_Z E_F-intensity map, normalized to the maximum intensity for each photon energy, showing the FS topology along P–X–P and the filling in of the hole-pocket with f-weight above resonance. Dashed arcs indicate the trajectories of the on- and off-resonance spectra.

The correlation of f-weight at E_F to the underlying d-band structure and Fermi surface, i.e. confinement to the center of a hole pocket, can be rationalized in the framework of Anderson lattice treatments (see for example Ref. [31]) involving renormalized hybridization of a renormalized f-level to d-states in the vicinity of a d-band E_F-crossing. We postpone an explication of this approach to interpreting the data to a later paper, but note that similar behavior is seen at the Γ and Z-points where the hole-pockets are smaller and the resonant f-weight seen in Fig. 3 is stronger. In addition, agreement with calculated high binding energy band dispersions indicates that the bulk band structure is being probed despite the surface sensitivity of the measurement. Surface effects, well established in cerium systems [15,16] but not in uranium systems [17], are not readily apparent in the current data.

3. SmB_6

SmB_6 offers an interesting contrast. Its mixed valence was clearly observed in early low-resolution photoemission spectra [32] showing final state atomic multiplet structure from $Sm^{2+}4f^6 \rightarrow 4f^5$ and $Sm^{3+}4f^5 \rightarrow 4f^4$ transitions, very near to E_F, and displaced ≈ 5 eV below E_F by the f-Coulomb energy, respectively. Transport properties [33] and optical spectra [34] show both a small gap $\approx$ 5–20 meV and states within the gap which may [35] be intrinsic. One class of gap-formation models invokes hybridization between Sm atomic 4f states and Sm 5d conduction band states [36,37], perhaps augmented by Kondo-type renormalization effects [38].

Fig. 5(a) is an intensity plot of SRC Scienta data at $h\nu = 70$ eV for the first 2.5 eV below E_F along the Γ–X line of the simple cubic Brillouin zone. It provides the first complete experimental overview of the essential ingredients of the SmB_6 electronic structure. The sharp

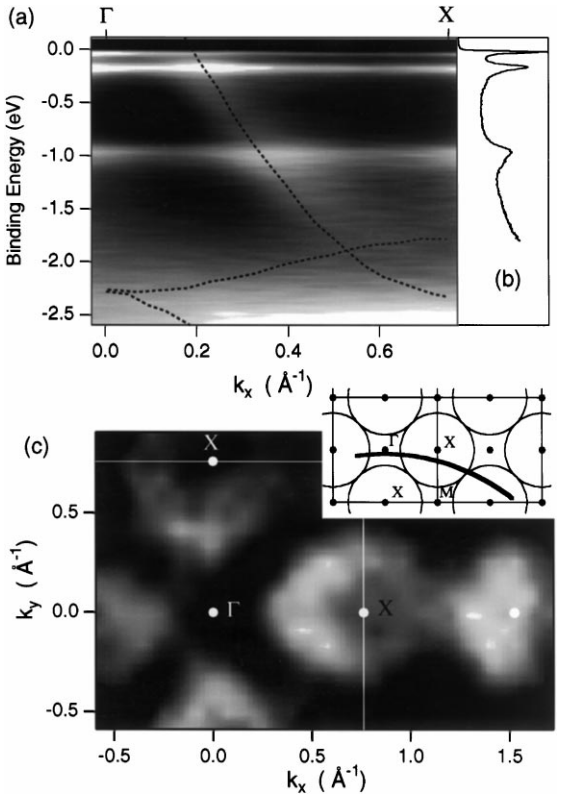

Fig. 5. (a) Intensity plot of spectra at 70 eV for SmB_6 showing a single parabolic d-band centered on X dispersing through k-independent Sm 4f-states. The dashed lines are calculated bands [39]. (b) High-resolution spectrum at 40 eV. (c) An E_F-intensity angular map at 26 eV cutting through four spherical pockets centered on X formed by the d-band dispersion shown in (a). The inset illustrates the X-pockets and the arc of the intensity map in the k_X–k_Z plane.

k-independent features, seen also in the $h\nu = 40$ eV spectrum of Fig. 5(b), at ≈ 0, -0.1 and near -1 eV arise from the $^6F_{5/2}$, $^6F_{7/2}$ and $^6H_{5/2}$, $^6H_{7/2}$ final state multiplets of the $4f^6 \rightarrow 4f^5$ transitions, respectively. A high-resolution line shape study shows an E_F gap or pseudogap with the $^6H_{5/2}$ peak at ≈ 16 meV below E_F, and RESPES shows also the $^6H_{9/2}$ and $^6H_{11/2}$ peaks at ≈ 0.3 and 0.47 eV. These details of the $4f^6 \rightarrow 4f^5$ transitions have not been observed before. The dispersing peak, which is also new, is in excellent agreement with band theory predictions for the single d-band (a band calculation for EuB_6 is used [39]). The E_F-intensity map of Fig. 5(c) shows the Fermi surface that would result if the d-band dispersion were not interrupted by whatever gap formation mechanism is operative. In particular, the parabolic d-band dispersion of Fig. 5(a) would form large circular electron-pockets centered on the X-points (see Fig. 5 inset). The E_F-intensity map at $h\nu = 26$ eV starts near Γ at normal emission and cuts in a hemispherical arc through four of these X-pockets in the first BZ and into the top of another one in the second BZ. Space limitations preclude detailed discussion of the data, but we draw attention to (a) the k-independence of the f-features, and apparent incoherence of the f and d features, in sharp contrast to the findings for URu_2Si_2, (b) the presence of the lowest energy $4f^6 \rightarrow 4f^5$ transition at roughly the gap energy from E_F, which speaks against the simplest Kondo scenario, and (c) the extreme broadness of the dispersing d-band, even near E_F, which suggests intense scattering due to the presence of the f-states.

In summary, we have presented spectra which portend bright new prospects for f-electron ARPES in a future which has just begun.

Acknowledgements

We would like to thank H. Yamagami for making available his band calculations prior to their publication. We also gratefully acknowledge the support of D.K. Shuh and N.M. Edelstein of the Actinide Chemistry Group, Lawrence Berkeley National Laboratory, in assisting with radioactive sample handling, H. Höchst for his support in using the SRC Scienta endstation, and L.-Z Liu for his contribution to the earliest phases of the work. This work was supported at University of Michigan by the U.S. DoE under Contract No. DE-FG02-90ER45416 and by the U.S. NSF Grant No. DMR-99-71611; and at UCSD by U.S. NSF Grant No. DMR-97-05454. The SRC is supported by the U.S. NSF Grant No. DMR-95-31009, and the ALS by the U.S. DOE under Contract No. DE-AC03-76SF00098.

References

[1] P.A. Lee, T.M. Rice, J.W. Serene, L.J. Sham, J.W. Wilkins, Comments Condens. Matter Phys. 12 (1986) 99.
[2] J.W. Allen, S.J. Oh, O. Gunnarsson, K. Schonhammer, M.B. Maple, M.S. Torikachvili, I. Lindau, Adv. Phys. 35 (1986) 275.
[3] D. Malterre, M. Grioni, Y. Baer, Adv. Phys. 45 (1996) 299.
[4] W.R. Johanson, G.W. Crabtree, A.S. Edelstein, O.D. McMasters, Phys. Rev. Lett. 46 (1981) 504.
[5] F.S. Tautz, S.R. Julian, G.J. McMullan, G.G. Lonzarich, Physica B 206–207 (1995) 29.
[6] Y. Onuki, Physica B 186–188 (1993) 92.
[7] A.B. Andrews, J.J. Joyce, A.J. Arko, J.D. Thompson, J. Tang, J.M. Lawrence, J.C. Hemminger, Phys. Rev. B 51 (1995) 3277.
[8] H. Kumigashira, S.H. Yang, T. Yokoya, A. Chainani, T. Takahashi, A. Uesawa, T. Suzuki, O. Sakai, Y. Kaneta, Phys. Rev. B 54 (1996) 9341.
[9] M. Garnier, K. Breuer, D. Purdie, M. Hengsberger, Y. Baer, B. Delley, Phys. Rev. Lett. 78 (1997) 4127.

[10] F.J. Himpsel, Adv. Phys. 32 (1983) 1.
[11] W. Bardyszewski, L. Hedin, Phys. Scripta 32 (1985) 439.
[12] T. Grandke, L. Ley, M. Cardona, Phys. Rev. B 18 (1978) 3847.
[13] M. Lindroos, A. Bansil, Phys. Rev. Lett. 77 (1996) 2985.
[14] J.W. Allen, in: R.Z. Bachrach (Ed.), Synchtrotron Radiation Research; Advances in Surface and Interface Science, Vol. 1, Techniques, Plenum, New York, 1992, p. 253.
[15] L.Z. Liu, J.W. Allen, O. Gunnarsson, N.E. Christensen, O.K. Andersen, Phys. Rev. B 45 (1992) 8934.
[16] L. Duo, Surf. Sci. Rep. 32 (1998) 233.
[17] J.W. Allen, Y.X. Zhang, L.H. Tjeng, L.E. Cox, M.B. Maple, C.T. Chen, J. Electron Spectrosc. Relat. Phenom. 78 (1996) 57.
[18] H. Kumigashira, T. Sato, T. Yokoya, T. Takahashi, S. Yoshii, M. Kasaya, Phys. Rev. Lett. 82 (1999) 1943.
[19] T. Warwick, P. Heimann, D. Mossessian, W. McKinney, H. Padmore, Rev. Sci. Instrum. 66 (1995) 2037.
[20] F.J. Himpsel, L.J. Terminello, D.A. Lapiano-Smith, E.A. Eklund, J.J. Barton, Phys. Rev. Lett. 72 (1992) 2757.
[21] P. Aebi, J. Osterwalder, P. Schwaller, L. Schlapbach, M. Shimoda, T. Mochiku, K. Kadowaki, Phys. Rev. Lett. 72 (1994) 2757.
[22] H. Nishimoto, T. Nakatani, T. Matsushita, S. Imada, H. Daimon, S. Suga, J. Phys.: Condens. Matter 8 (1996) 2715.
[23] J. Osterwalder, Surf. Rev. Lett. 4 (1997) 391.
[24] M.B. Maple, J.W. Chen, Y. Dalichaouch, T. Kohara, C. Rossel, M.S. Torikachvili, M.W. McElfresh, J.D. Thompson, Phys. Rev. Lett. 56 (1986) 185.
[25] T.T.M. Palstra, A.A. Menovsky, J. van den Berg, A.J. Dirkmaat, P.H. Kes, G.J. Nieuwenhuys, J.A. Mydosh, Phys. Rev. Lett. 55 (1985) 2727.
[26] G. Zwicknagl, Adv. Phys. 41 (1992) 203.
[27] H. Yamagami, private communication, 1998.
[28] M.R. Norman, T. Oguchi, A.J. Freeman, Phys. Rev. B 38 (1988) 11193.
[29] G.J. Rozing, P.E. Mijnarends, A.A. Menovsky, P.F. de Châtel, Phys. Rev. B 43 (1991) 9523.
[30] N. Keller, S.A.J. Wiegers, J.A.A.J. Perenboom, A. de Visser, A.A. Menovsky, J.J.M. Franse, J. Magn. Magn. Mater. 177–181 (1998) 298.
[31] A.N. Tahvildar-Zadeh, M. Jarrell, J.K. Freericks, Phys. Rev. Lett. 80 (1998) 5168.
[32] J.N. Chazalviel, M. Campagna, G.K. Wertheim, P.H. Schmidt, Phys. Rev. B 14 (1976) 4586.
[33] J.W. Allen, B. Batlogg, P. Wachter, Phys. Rev. B 20 (1979) 4807.
[34] B. Gorshunov, N. Sluchanko, A. Volkov, M. Dressel, G. Knebel, A. Loidl, S. Kunii, Phys. Rev. B 59 (1999) 1808.
[35] J.C. Cooley, M.C. Aronson, Z. Fisk, P.C. Canfield, Phys. Rev. Lett. 74 (1995) 1629.
[36] N.F. Mott, Philos. Mag. 30 (1974) 403.
[37] R.M. Martin, J.W. Allen, J. Appl. Phys. (USA) 50 (1979) 7561.
[38] A.J. Millis, in: E. Manousakis (Ed.), Addison–Wesley, Menlo Park, 1992, p. 146.
[39] S. Massidda, A. Continenza, T.M. De Pascale, R. Monnier, Z. Phys. B 102 (1997) 83.